crystals

MDPI

Article

Improvement of Hydrogenation and Dehydrogenation Kinetics of As-Cast AZ91 Magnesium Alloy via Twin Parallel Channel Angular Extrusion Processing

Mohammad Abdi [1], Ramin Ebrahimi [1,*] and Ebad Bagherpour [2]

[1] Department of Materials Science and Engineering, School of Engineering, Shiraz University, Shiraz 71348-51154, Iran
[2] Brunel Centre for Advanced Solidification Technology (BCAST), Brunel University London, Uxbridge, Middlesex UB8 3PH, UK
* Correspondence: ebrahimy@shirazu.ac.ir

Abstract: In the current study, Twin Parallel Channel Angular Extrusion (TPCAE) as a developed SPD processing technique is used to improve the hydrogen storage properties of AZ91 cast alloy. The processing is conducted at different temperatures, ranging from 340 °C down to 200 °C. The hydrogen absorption and desorption tests are conducted kinetically at three different temperatures, using a Sievert-type apparatus. Remarkable improvement in the absorption kinetic is achieved as a result of the TPCAE processing. A maximum absorption capacity of 6.1 wt.% within a time span of 2000 s is achieved for the sample with three passes of processing complemented at 250 °C. Also, the kinetic of dehydrogenation is improved significantly and complete desorption at 350 °C is achieved for all the processed samples within a time span of maximum 2500 s. By calculating the activation energy of hydrogenation and evaluating the microstructure changes, it is found that implementing sufficient thermomechanical work level along with applying the last pass of the process at lower temperature results in a reduction of the activation energy and improvement of the hydrogenation kinetic.

Keywords: AZ91 magnesium alloy; severe plastic deformation; hydrogen storage; kinetic

check for updates

Citation: Abdi, M.; Ebrahimi, R.; Bagherpour, E. Improvement of Hydrogenation and Dehydrogenation Kinetics of As-Cast AZ91 Magnesium Alloy via Twin Parallel Channel Angular Extrusion Processing. *Crystals* **2022**, *12*, 1428. https://doi.org/10.3390/cryst12101428

Academic Editor: Mingyi Zheng

Received: 15 September 2022
Accepted: 6 October 2022
Published: 9 October 2022

Publisher's Note: MDPI stays neutral with regard to jurisdictional claims in published maps and institutional affiliations.

Copyright: © 2022 by the authors. Licensee MDPI, Basel, Switzerland. This article is an open access article distributed under the terms and conditions of the Creative Commons Attribution (CC BY) license (https://creativecommons.org/licenses/by/4.0/).

1. Introduction

Nowadays, fossil fuels have caused significant problems, including global warming and climate change. Hydrogen can be considered as an alternative energy resource, especially in the automotive industry and future energy systems due to its safety, abundance, and cleanness [1]. However, extensive use of hydrogen is hindered by its storage difficulties. Storage in the solid state via metal hydrides presents advantageous features, such as high gravity storage capacity and safety [2]. Mg is an attractive material in new research areas such as the ion battery, hydrogen storage, and biomaterials due to the lightness, recyclability, corrosion resistance, and low cost [3]. In the case of hydrogen storage, Mg has a high gravimetric capacity (7.6 wt.%) and has the potentiality to be used for onboard vehicular applications [1]. Nonetheless, there are major problems with the vast mobile application of MgH_2, including poor kinetics of absorption/desorption of hydrogen and high stability of MgH_2, leading to increase its dissociation temperature [1]. The poor kinetics are mainly due to the low diffusivity of hydrogen in the Mg crystalline lattice and the presence of thick surface oxide layer hindering H_2 dissociation and penetration of H atoms into the bulk [4].

In this regard, research works have been performed to improve the hydrogenation performance of Mg. From the thermodynamic viewpoint, alloying with other elements, such as Al, decreases the hydrogen binding energy [5,6]. Although Al does not participate in the hydrogen absorption, it can destabilize MgH_2 and improve desorption efficiency [7]. Catalytic additions (Pd, Fe, V, Ni, Ti, and Nb_2O_5) to the Mg matrix have been reported to enhance H_2 dissociation and improve hydrogenation kinetic [8]. Moreover, the kinetic

of hydrogen storage can be improved significantly by refining the microstructure and producing a high fraction of structural defects, such as vacancies, dislocations, and grain boundaries with low activation energy of diffusion [9]. These defects, especially high angle grain boundaries, can act as straightforward paths for diffusion and absorption of hydrogen atoms into the Mg bulk [10].

High energy ball milling (HEBM) [1,11] is a conventional method used vastly to make nanostructure materials consisting of ultrafine grains and lattice defects, which can significantly improve the hydrogenation kinetic. However, HEBM has some limitations, including high contamination, intensive air reactivity causing fire hazard, and high energy consuming and/or high cost for production of small quantities [12]. From this perspective, these limitations would be addressed by bulk processing using severe plastic deformation (SPD), in which intensive strain is accumulated by repetition of plastic deformation [13]. By applying SPD, ultrafine grain (UFG) structures are obtained in favor of the diffusion of hydrogen atoms, which in turn avoids contamination and fire risk.

Mg and its alloys are of limited workability due to the lack of sufficient active slip systems in the hexagonal structure and their SPD processing is challenging. Nonetheless, some strategies can be considered to overcome these challenges. Some of these include applying SPD at high temperatures to activate the pyramidal slip systems, increasing the die angles to reduce the strain localized points, and using backward pressure [14]. Also, some other works such as prestraining or developing a texture have been conducted to improve the formability and mechanical behavior of Mg alloys [15]. Recently, investigations were conducted to study the ability of various SPD techniques, including equal channel angular extrusion (ECAE) [7,16–18], high-pressure torsion (HPT) [19,20], and accumulative roll bonding (ARB) [21] in improvement of the hydrogen storage properties of Mg-based alloys. Skripnyuk et al. pioneered the use of ECAE for the purpose [22,23]. They also investigated a combination of the ECAE and HEBM processes to improve the kinetic properties of the ZK60 alloy and achieved the absorption capacity of 6.2 wt.% at 300 °C [23]. Asselli et al. [24] used both ECAE and ARB to improve the hydrogenation behavior of ZK60 alloy, on the increase of the maximum storage capacity from 4.77 wt.% (by only ECAE processing) up to 6.4 wt.% (by combination of ECAE and ARB processing). Botta et al. [25] investigated the processing effect of HPT and cold rolling, separately, to improve the absorption properties of bulk Mg samples. They were also successful in increase of maximum absorption capacity of pure Mg ribbons produced by melt spinning for almost 65% due to the formation of a strong (0001) texture during cold rolling. Texture effects, formed during rolling, on the improvement of hydrogenation kinetics of pure Mg and its alloys, AZ91 and AM60D, were also reported in other studies [21,26]. Furthermore, Huot et al. [27] have reported the different effects of ECAE processing routes in improving hydrogenation kinetics of Mg alloys. In this regard, using processing route of A (in which the sample is pressed repetitively without rotation) in ECAE delivers a very marked texture for AZ31 Mg alloy, while using route Bc (in which the sample is rotated by 90° in the same sense between each pass) prepares more grain refinements with random texture. Both processing routes deliver samples with the ability to uptake hydrogen up to 7.6 wt.%. However, the samples processed by route A show an incubation time before start of hydrogenation, while the ones processed by route B_c start the hydrogenation readily without any incubation time.

The main drawback of SPD processing is that they have not been industrialized so far. The current study addresses the feasibility of using a novel developed SPD technique, named twin parallel channel angular extrusion (TPCAE), which is one step closer to be industrialized in comparison to the conventional SPD ones, especially in the hydrogen storage application. TPCAE is a developed technique of ECAE in parallel channels, in which less energy per volume of material is consumed, while the tool has much more stability [28]. As cast AZ91 alloy was selected as the hydrogen storage material due to the existence of Al which decreases the hydrogen binding energy and destabilizes the MgH_2 hydride phase. Considering a solution treatment and quenching in water as a preliminary step, TPCAE at a temperature higher than 300 °C was started and continued

for several passes by a step-by-step reduction of temperature to 200 °C in different ways. Then, hydrogenation kinetics were measured for different processing conditions. Moreover, the effect of processing route and thermomechanical work level on the hydrogen storage properties of AZ91 alloy were evaluated considering the activation energy concept.

2. Materials and Methods

For TPCAE processing a commercial cast AZ91 Mg alloy was used with the chemical composition illustrated in Table 1.

Table 1. Chemical composition of the AZ91 alloy in wt.%.

Mg	Al	Zn	Mn	Fe	Si	Cu	Ca
Base	8.9	0.85	0.338	0.01	0.08	0.004	0.04

Prior to the processing, a solution heat treatment consisting of homogenization at 430 °C for 10 h and quenching in water was conducted. Afterward, the TPCAE processing in six different configurations, summarized in Table 2, was conducted.

Table 2. Different processing route for SPD of AZ91 alloy by TPCAE method.

Sample	Pass 1	Pass 2	Pass 3	Pass 4
S1	340 °C	-	-	-
S2	340 °C	300 °C	-	-
S3	340 °C	250 °C	-	-
S4	340 °C	200 °C	-	-
S5	340 °C	300 °C	250 °C	-
S6	340 °C	300 °C	250 °C	200 °C

Dislocation density was evaluated based on the modified Williamson–Hall approach, using X-ray diffraction (XRD) patterns of the processed samples. Mean grain size and volume fraction of precipitates were calculated using ImageJ software [29]. More detail on the material, the processing, and the calculations can be found in Ref. [30], published by the current authors.

One of the key factors to improve the hydrogenation properties of Mg alloys is to enhance the area-to-mass ratio of the material to facilitate the H_2 dissociation and penetration of H atoms into the bulk of material [31]. As a result, powders of the processed samples were needed for the investigations. Therefore, the samples were made into powder using a filing process under controlled argon atmosphere to prevent the formation of the thick surface-oxide layer on the powder surface. The activation process was conducted with the following details:

- For each test, 0.22 g powder was placed in the reactor and washed with hydrogen gas, followed by vacuuming to 10^{-2} mbar. The washing process was repeated three times.
- Afterward, it was placed under a highly enhanced vacuum condition with a pressure of 10^{-5} mbar. Then, the temperature was increased up to 150 °C. As the temperature increased, followed by the increase in the pressure, the vacuum pump worked for one hour to achieve the pressure of 10^{-5} mbar at 150 °C.
- Similar procedure was repeated as the temperature increased from 150 °C to 250 °C and from 250 °C to 350 °C, respectively, and the pressure was maintained at 10^{-5} mbar at the end of each temperature-rise step.
- Afterwards, hydrogen gas was injected into the sample at 350 °C under 30 bar pressure, and kept for 15 h.
- In the last stage, the sample powder was placed again under a vacuum of 10^{-5} mbar at 350 °C.

After the activation process, the kinetic measurement of absorption was started at 350 °C by the injection of hydrogen gas at 30 bar following by the desorption measurement at a pressure of 10^{-1} mbar. To perform the test at 300 °C, there was a need to ensure that all the hydrogen atoms are brought to the gas phase. Thus, the vacuum pump worked to lower the pressure down to 10^{-5} mbar, while the reactor temperature was set to 300 °C. Then, the absorption/desorption measurements were repeated at this temperature in a similar condition to that of 350 °C. The same procedure was repeated for the temperature of 250 °C. Hydrogenation and dehydrogenation measurements were conducted according to the same procedure for all samples obtained through the different TPCAE processing conditions, as specified in Table 2. The analysis of XRD was performed after hydrogenation and dehydrogenation, using Cu-Kα peak with the wavelength of 0.154056 nm, a time scale of 1 s, a length scale of 0.05° and an angle range of 20–100°.

3. Results

3.1. Microstructure Evolution

Thermomechanical processing of the solution heat-treated AZ91 alloy results in a remarkable microstructure evolution. Table 3 illustrates the variation of mean grain size, dislocation density, and volume fraction of precipitate (β-$Mg_{17}Al_{12}$ phase) during different conditions of processing. The determinations can be found elsewhere [30].

Table 3. Microstructure evolution for the TPCAE processed samples of AZ91 alloy via different processing routes [30].

Sample	Mean Grain Size (μm)	Dislocation Density ($\times 10^{14}/m^2$)	Volume Fraction of β-Phase Precipitate (%)
As cast	550	0.1 [32]	-
S1	13.54	2.73	3
S2	4.29	1.33	8.7
S3	2.39	0.36	13.3
S4	5.67	4.1	15.3
S5	2.19	0.61	15.4
S6	3.66	3.28	15.6

The primary as cast grain size is reduced via one pass of processing at 340 °C. It should be mentioned that recrystallization and precipitation happen simultaneously during plastic deformation [30]. Precipitation occurs during the processing, owing to the fact that the β phase was eliminated through the solution treatment before the processing, resulting in a supersaturated microstructure. Therefore, there is a potential for precipitation of β phase through the TPCAE processing [33].

By lowering the temperature of the second pass down to 300 °C (S2 sample) and 250 °C (S3 sample), more grain refinement is achieved and precipitation of β phase is enhanced, while the dislocation density is reduced, indicating the dominance of recrystallization. Moreover, at lower temperature the diffusion rate decreases, leading to the prevention of grain growth and retard of precipitate coarsening. Thereby, the fine and dispersed precipitates prevent growth of new recrystallized grains via the pinning effect mechanism [34]. By reducing temperature of the second pass to 200 °C (S4 sample), recrystallization is replaced by twinning, which occurs in the un-recrystallized grains remaining from the first pass of processing at 340 °C [35]. In this condition, the dislocation density increases by one order of magnitude, as compared to the S3 sample.

By increasing level of the thermomechanical processing applied through the step-by-step reduction of the processing temperature, the mean grain size decreases to its lowest size of 2.19 μm (S5 sample). Besides, the volume fraction of β-phase precipitate increases in comparison with the S3 sample and reaches the level of 15.4%. The observed increase of β phase by increasing the accumulative strain is in accordance with the previous report

of Huang et al. [7], on the improvement of the hydrogenation behavior of AZ61 alloy by ECAE.

Interestingly, by comparing S5 and S6 samples, an increase in the grain size is observed. The reason is the coarsening of the of the small precipitates due to the further thermomechanical processing which in turn, would lead to the grain coarsening because of the slight weakening of the pinning effect mechanism [33]. On the other hand, the fraction of β-phase precipitate remains almost constant in S4, S5, and S6 samples, indicating that the subsequent thermomechanical processing does not have any significant effect on the fraction of the precipitates after the second pass of the TPCAE; instead, more dispersion of this phase occurs, resulting in a more uniform distributed microstructure [30,33].

3.2. Hydrogen Absorption and Desorption Properties

The absorption and desorption kinetic measurements at 350 °C, 300 °C, and 250 °C are shown for the cast sample in Figure 1. The maximum absorption capacity is about 2.5 wt.%. The hydrogenation kinetic becomes slower by decreasing the temperature. The dehydrogenation is incomplete at all temperatures. However, dehydrogenation kinetic at 350 °C is significantly better, as compared to the lower temperatures.

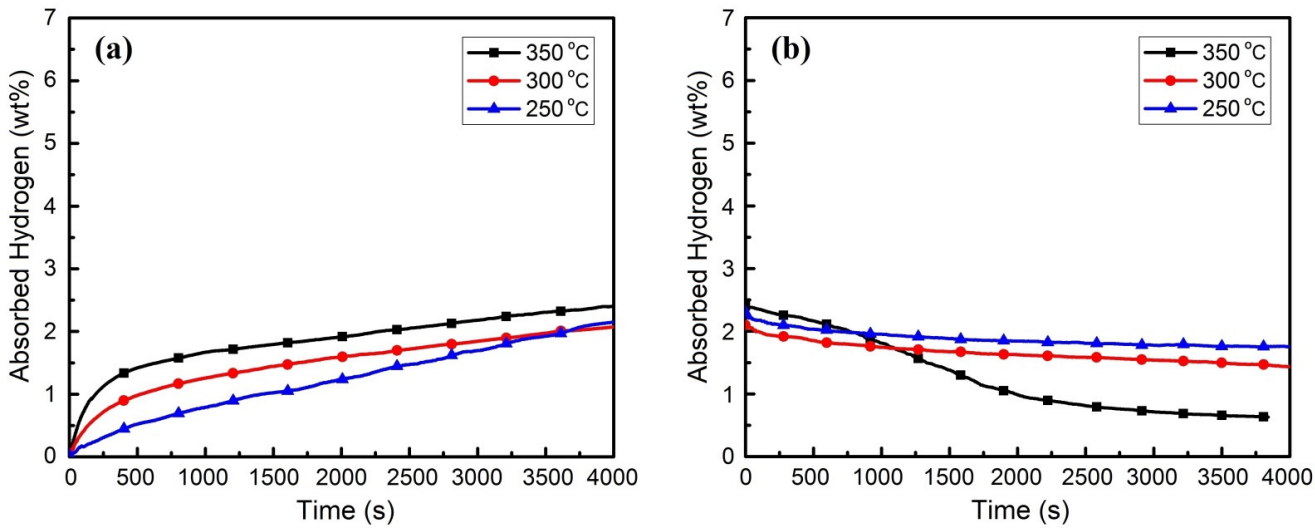

Figure 1. Kinetic of hydrogenation and dehydrogenation for as cast AZ91 alloy at different temperatures: (**a**) Hydrogenation at pressure of 30 bar; (**b**) Dehydrogenation at pressure of 10^{-1} mbar.

Hydrogenation and dehydrogenation behaviors for the S1 and S2 samples are illustrated in Figure 2. As shown in Figure 2a, a single pass of the TPCAE improves the maximum absorption capacity at 350 °C significantly from 2.5% to 4.8 wt.%, as well as a significant enhancement in the hydrogenation kinetics. In addition, for the S1 sample, the hydrogenation trend at 300 °C tends to get considerably close to that at 350 °C, but the kinetic is not as fast as that. Thermomechanical processing does not improve the absorption trend at 250 °C. From Figure 2b it is obvious that a single pass of TPCAE was enough to ensure the complete desorption at 350 °C with a suitable kinetic. However, the dehydrogenation kinetics are significantly slower at lower temperatures. The improvements in absorption could be associated with the considerably lower grain size and the higher dislocation density of the sample after a pass of TPCAE at 340 °C.

After the second pass of TPCAE at 300 °C, the maximum absorption capacity reaches the level of 5.5 wt.% at 350 °C (see Figure 2c). The maximum absorption decreases to about 4.6 wt.% by decreasing the hydrogenation temperature to 300 °C. However, the kinetic of absorption within the first 250 s is higher at 300 °C. Furthermore, a second pass of TPCAE improves the absorption behavior at 250 °C, it can be realized by comparing the absorption behavior of S1 and S2 samples in Figure 2a,c, respectively. The desorption behavior of the

S2 sample has a similar trend and kinetic to the S1 (Figure 2d), so that a complete desorption is achieved at 350 °C, while for the lower temperature the kinetics are still very poor.

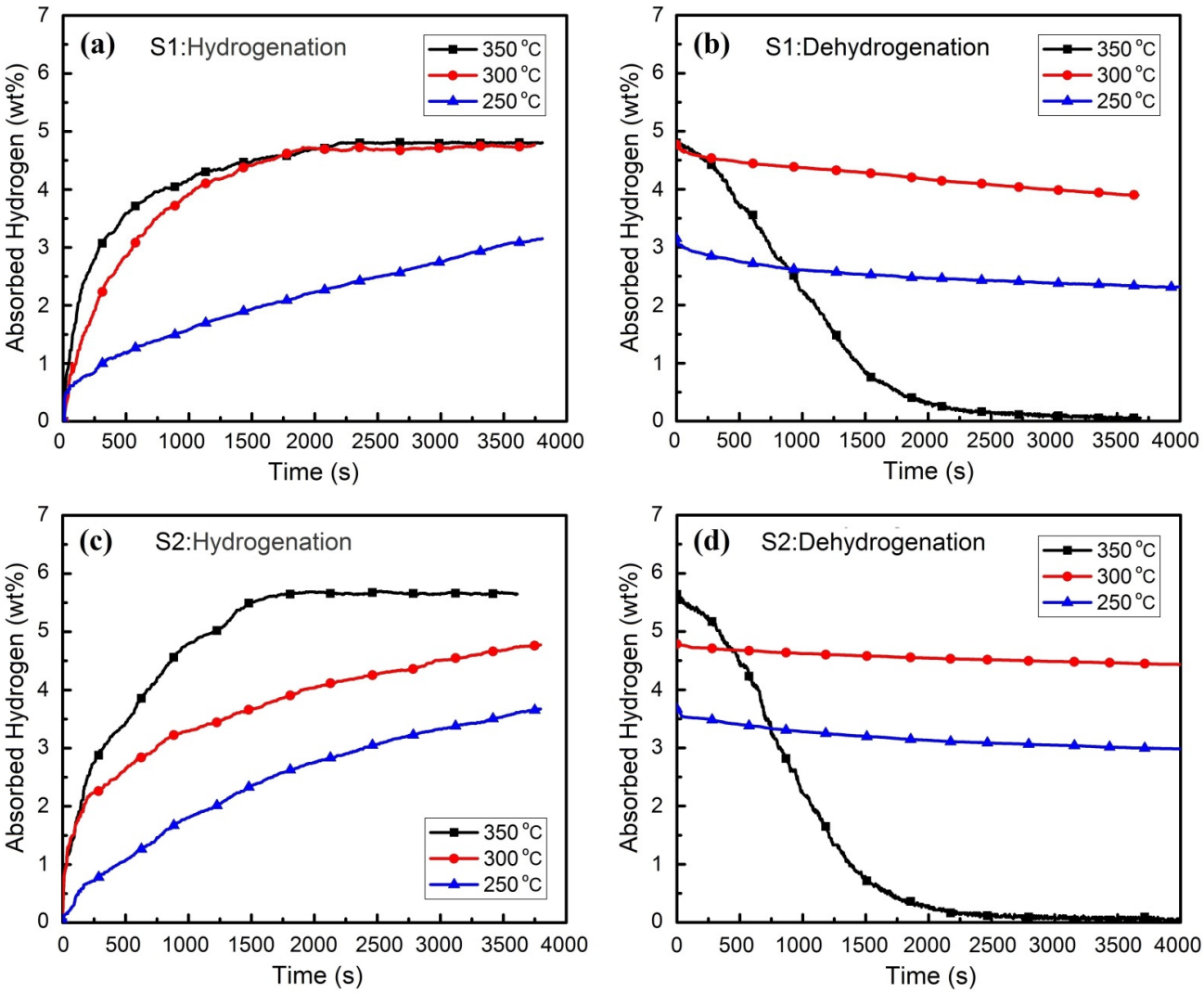

Figure 2. Hydrogenation kinetics at 30 bar and dehydrogenation kinetics at 10^{-1} mbar for different temperatures. (**a**,**b**) S1 sample (a pass of TPCAE at 340 °C), (**c**,**d**) S2 sample (second pass of TPCAE at 300 °C).

Hydrogenation and dehydrogenation kinetics for the S3 and S4 samples are illustrated in Figure 3. Clearly, lowering the second pass processing temperature from 300 °C to 250 °C, makes a huge improvement in hydrogenation by equalizing the hydrogenation trend for all the three temperatures while still the maximum absorption of 5.5 wt.% is achieved at 350 °C. Whereas the maximum absorption at 250 °C for the S2 sample was 3.4 wt.%, it is 4.3 wt.% for the S3 sample, which shows almost 27% increase in the maximum absorption for the lowest hydrogenation temperature. Considering Figure 3b, the dehydrogenation of S3 sample at 350 °C is fully complemented below 1000 s which is much shorter time in comparison with S1 and S2 samples. Comparing the dehydrogenation kinetic of S2 and S3 samples (see Figures 2d and 3b), it is clear that the dehydrogenation kinetic at 300 °C is improved slightly in S3 sample, while at 250 °C no significant improvement is observed. The improvement of hydrogenation/dehydrogenation behavior of the sample processed by two passes of TPCAE in lower temperature is attributed to the higher level of recrystallization occurring at the lower temperatures during the processing, which leads to

the formation of a highly refined microstructure with higher fraction of sub-structures and grain boundaries.

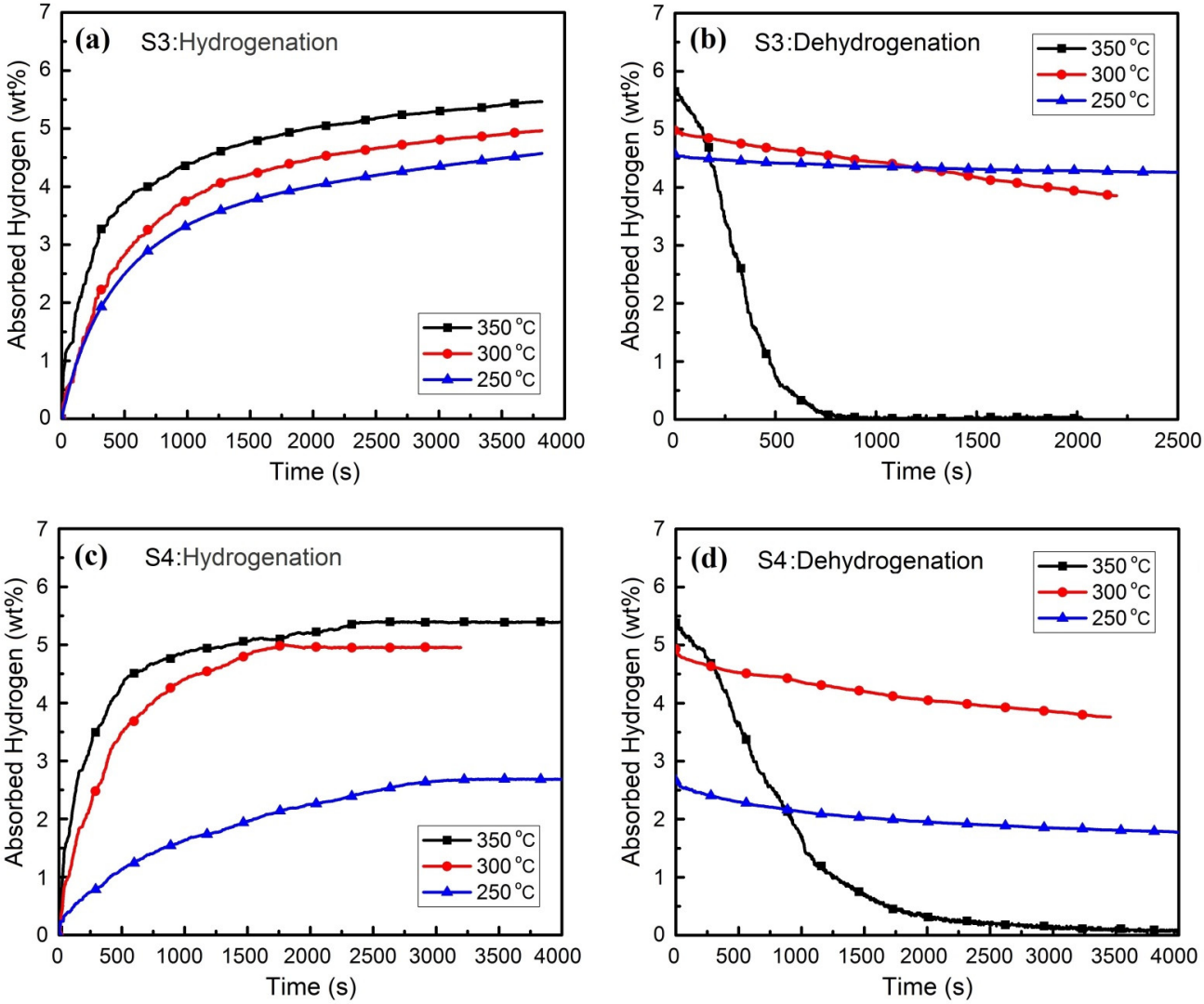

Figure 3. Hydrogenation kinetics at 30 bar and dehydrogenation kinetics at 10^{-1} mbar for different temperatures: (**a**,**b**) S3 sample (second pass of TPCAE at 250 °C); (**c**,**d**) S4 sample (second pass of TPCAE at 200 °C).

Further reduction in the TPCAE processing temperature to 200 °C (S4 sample), does not have any effect on the maximum absorption capacity at 350 °C (see Figure 3c) and it is almost same as what is achieved for S3 sample. In addition, the hydrogenation trend of S4 sample at 300 °C is comparable to that of 350 °C. Nevertheless, unlike S3 sample, the hydrogenation trend of S4 sample at 250 °C suffers from a considerable drop. Comparing the dehydrogenation of S4 sample at 350 °C (Figure 3d) with S3 sample (Figure 3b) shows a considerable increase in the complementation time. The weakening of hydrogenation and dehydrogenation for the sample having a lower TPCAE processing temperature can be described by the existence of a bimodal microstructure [30] originated from activation of twinning mechanism instead of recrystallization in the second pass of the processing at lower temperatures. It is concluded that, for the second pass of the TPCAE, processing at 250 °C (in which recrystallization is the dominant mechanism) results in the best absorption and desorption behavior.

To investigate the effect of hydrogenation and dehydrogenation on the phase transformation, XRD patterns of S4 after hydrogenation and dehydrogenation at 350 °C are illustrated in Figure 4, as examples. New diffraction peaks corresponding to MgH_2 phase are observed after hydrogenation, indicating the formation of a hydride phase. Also, peaks of aluminum appear after hydrogenation, as a result of transformation of the $Mg_{17}Al_{12}$ phase to Mg_2Al_3 and MgH_2, following by a transformation of Mg_2Al_3 to MgH_2 and Al [36,37]. Since still small Mg peaks exist, it shows the hydrogenation process is not completed (Figure 4a). On the other hand, as seen in Figure 4b, almost all of MgH_2 peaks disappear after desorption that indicates the approximately complete dehydrogenation at this temperature. Because of the reverse reactions, including the transformation of Al and MgH_2 to Mg_2Al_3, and then, Mg_2Al_3 and MgH_2 to $Mg_{17}Al_{12}$ phase, there are no Al peaks after dehydrogenation.

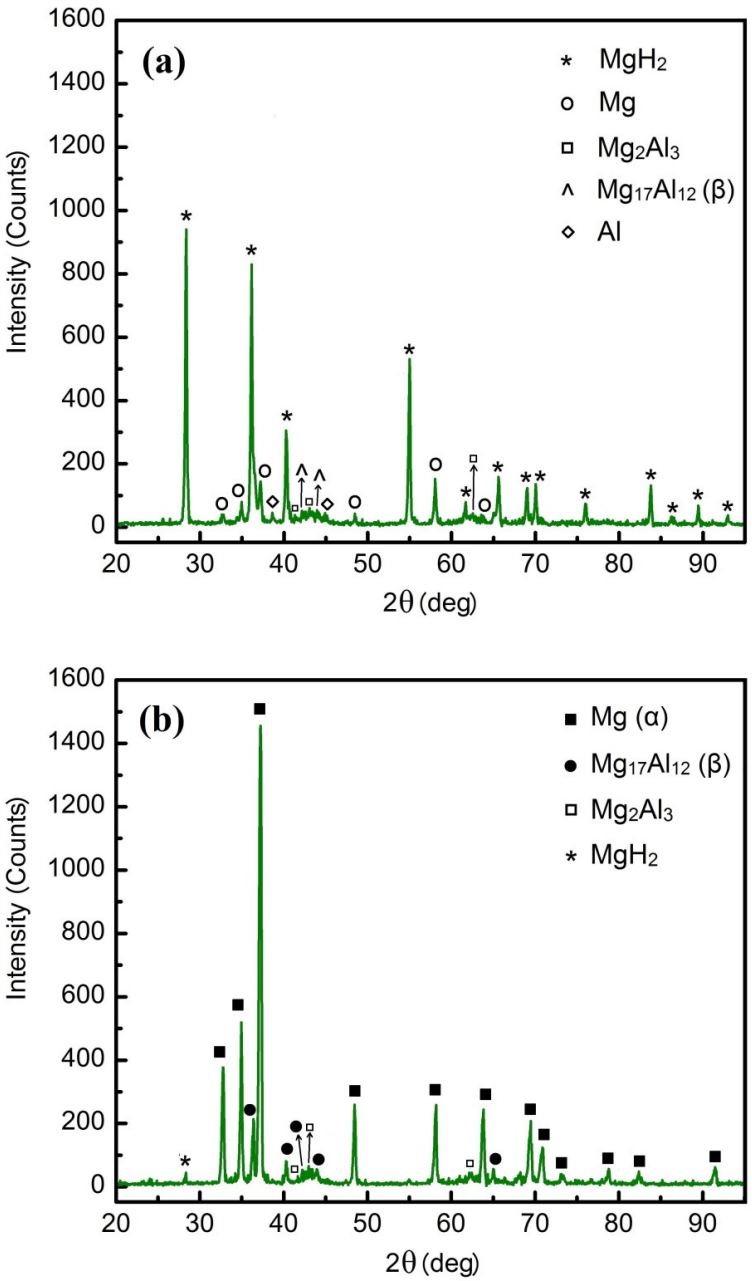

Figure 4. XRD diffraction patterns for S4 sample (second pass of TPCAE at 200 °C): (**a**) after hydrogenation; (**b**) after dehydrogenation.

The hydrogenation and dehydrogenation behaviors for the samples processed by three and four passes of TPCAE are illustrated in Figure 5. After the third pass of TPCAE, the maximum absorption capacity reaches its highest value of 6.1 wt.% (Figure 5a). Looking at the existing literature, reaching a level of 6.1 wt.% absorption capacity in this alloy using only a single SPD method is a significant achievement. For example, in 2017, Jorge et al. [21], has achieved a much lower amount of 4.5 wt.% by means of a combination of the ECAE and ARB processes without sample powdering. In another research, Floriano et al. [38] have managed to increase the hydrogen absorption capacity to 5.5 wt.% by performing low temperature rolling. The closest achieved maximum absorption capacity to the current research, has been reported by Amira et al. [39] in 2012, where the same level of hydrogen absorption capacity (6.1 wt.%) has been attained by a high energy ball milling.

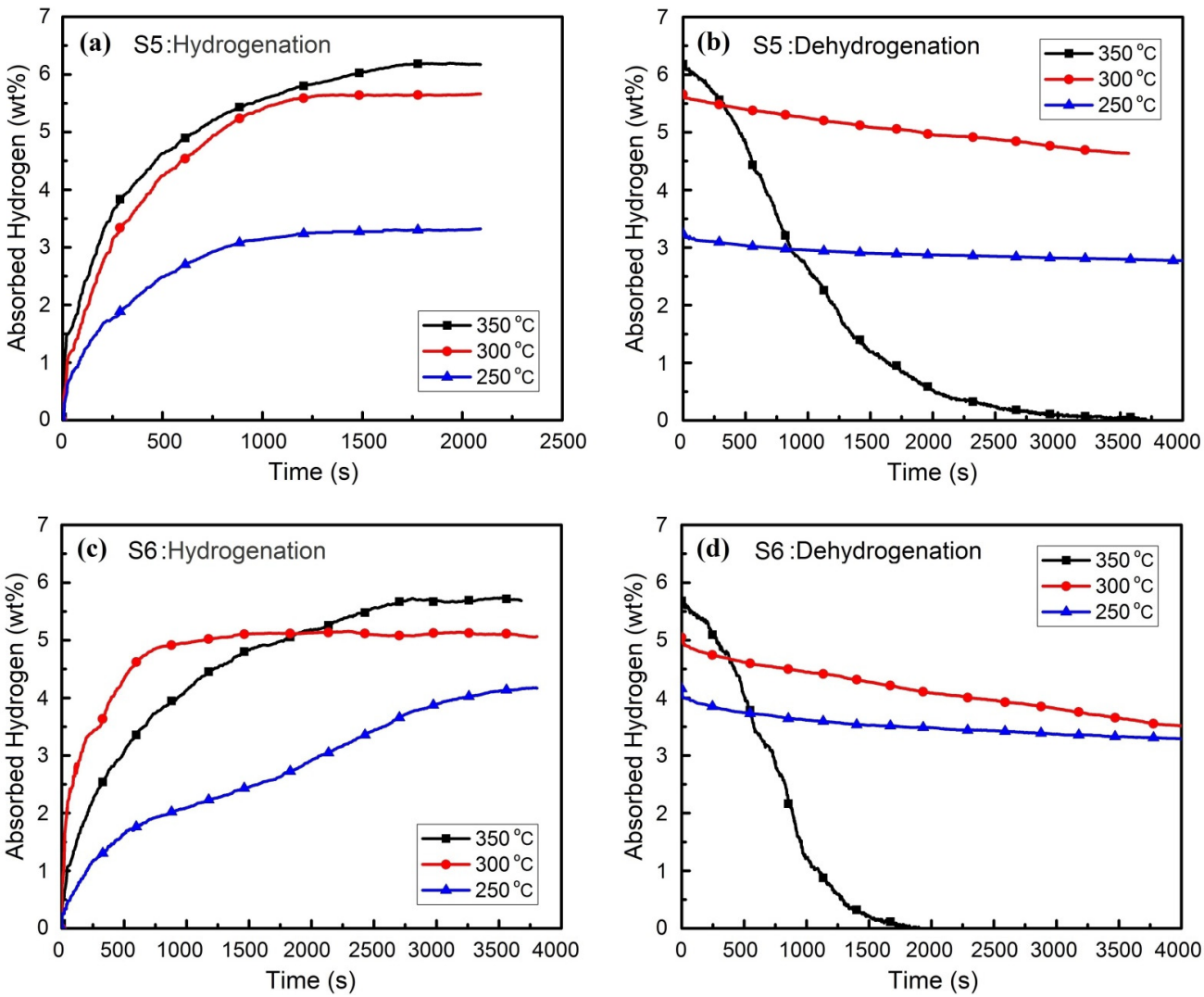

Figure 5. Hydrogenation kinetics at 30 bar and dehydrogenation kinetics at 10^{-1} mbar for different temperatures: (**a**,**b**) S5 sample (third pass of TPCAE at 250 °C); (**c**,**d**) S6 sample (fourth pass of TPCAE at 200 °C).

The hydrogenation kinetic for the S5 sample at 300 °C and at 350 °C is similar. At 250 °C, the maximum absorption after the third pass of TPCAE is about 3.3 wt.% which is lower than that 4.3 wt.%, which was achieved after the second pass of TPCAE (S3 sample), but the three passes deformed sample reaches its maximum capacity more quickly, which confirms the enhanced kinetic of the hydrogenation process at 250 °C. After the third pass of TPCAE (Figure 5b), full desorption of the sample is achieved at 350 °C with a longer time

span in comparison to the sample after the second pass of TPCAE at 250° C (Figure 3b). By comparing the dehydrogenation kinetic of S5 sample (Figure 5b) with S4 sample (Figure 3d), it is obvious that the trend is almost identical at all temperatures.

As seen in Figure 5c, the fourth pass of the TPCAE (S6 sample) decreases the absorption capacity of the sample at 350 °C while it improves the hydrogenation kinetic at 300 °C. However, the maximum absorption capacity at 250 °C is improved after the fourth pass of TPCAE and reached to the best achievable one which was observed in S3 sample (compare Figure 5c with Figure 3a). Likewise, the dehydrogenation kinetic of S6 sample (Figure 5d) is close to that of S3 (Figure 3b).

It can be said that in all the processed samples, a significant improvement for hydrogenation behaviors, especially at 350 °C and 300 °C, and dehydrogenation behaviors at 350 °C is achieved, in comparison to the as cast sample. This is due to the increase of internal defects, especially grain boundaries, during TPCAE processing which act as the pathways for diffusion of hydrogen atoms and nucleation sites for hydride phase transformation. As mentioned in Table 3, the mean grain size is reduced from 550 μm for the as cast sample to the range of 2.19-13.54 μm for the TPCAE processed samples.

It is worth noting that twin boundaries cannot be as effective as grain boundaries for the diffusion of hydrogen atoms due to the lack of amorphous regions at the twin planes [40]. Therefore, the twinning mechanism is not beneficial as much as recrystallization for hydrogenation and dehydrogenation behaviors.

4. Discussion

To comprehensively evaluate the effect of TPCAE processing routes on the Hydrogenation of the AZ91 alloy, it is important to consider the kinetic of hydrogenation thoroughly, in respect of the nucleation and the growth of the transformed hydride phase. Generally, the formation of a hydride phase from a metal base is a complex process. Typically, it can be divided into four simplified reactions [41]: (i) dissociation/adsorption of the H_2 molecules; (ii) surface penetration of the H atoms; (iii) bulk diffusion of the H atoms; (iv) hydride formation. In this regard, Johnson–Mehl–Avrami (JMA) equation has been proven very versatile in explaining the hydrogenation kinetic of a variety of metal-hydrogen systems. Considering this approach, the transformed fraction of hydride phase (α) is given vs. time (t) as:

$$\alpha = 1 - exp\{-(kt)^n\} \tag{1}$$

where k is the kinetic rate constant (nucleation and growth rates) and n is referred to as the Avrami exponent describing the type of nucleation and the growth dimensionality [42]. By taking the natural logarithm of both sides of Equation (1), it becomes:

$$ln[-ln(1-\alpha)] = lnk + n\ lnt. \tag{2}$$

Considering $ln\ k$ as the intersection of a linear curve with the vertical axis, the kinetic rate constant can be obtained. The kinetic rate constant varies with temperature in the Arrhenius form, as [21]:

$$k = k_o exp(-Q/RT) \tag{3}$$

where Q is the apparent activation energy, T is the temperature, R is the gas constant, and k_o is a constant independent from temperature. By plotting the lnk versus $1/T$, the apparent activation energy is found from the slope of linear regression. The calculations for S4 are illustrated in Figure 6, as an example.

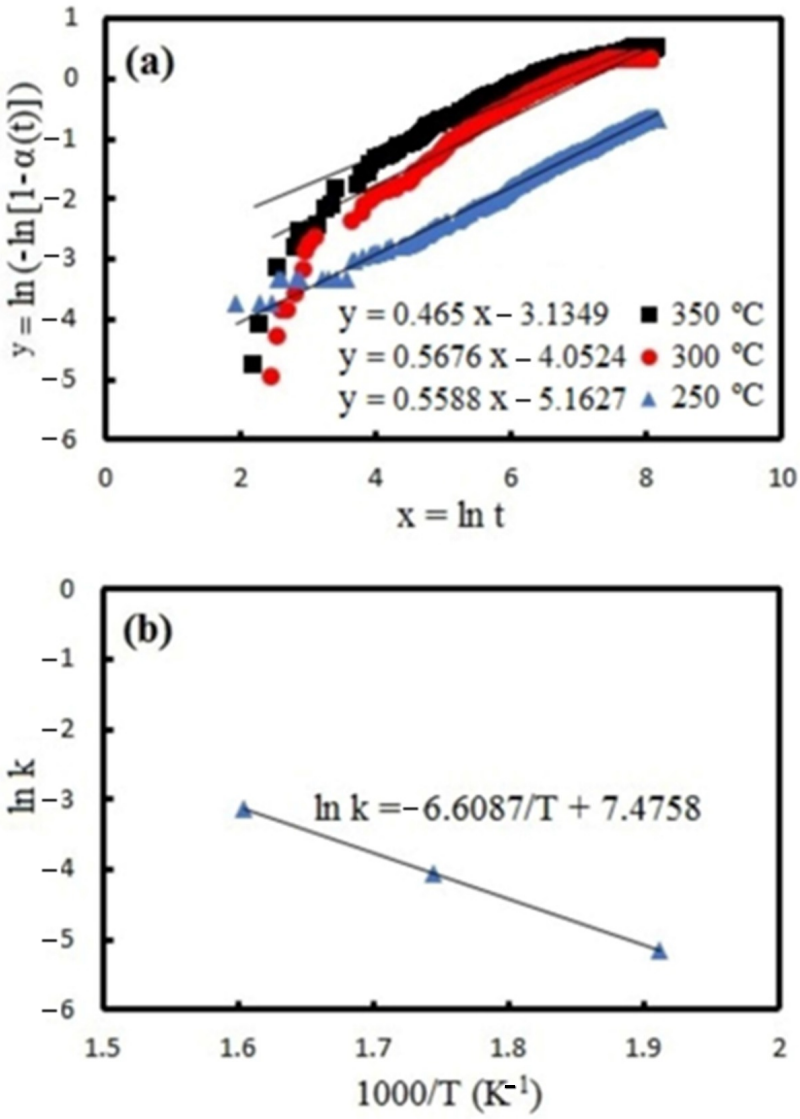

Figure 6. Determination of apparent activation energy (Q) for S4 sample (second pass of TPCAE at 200 °C): (**a**) plotting $ln[-ln(1-\alpha)]$ vs. lnt at different temperatures; (**b**) Arrhenius plot of the kinetic rate constants.

The kinetic parameters obtained by the JMA equation using the kinetic data are given in Tables 4 and 5 for all tested samples.

Table 4. Avrami exponent of the JMA model during hydrogenation of different samples at various temperatures.

Sample	n_{250}	n_{300}	n_{350}
As cast	0.73	0.48	0.39
S1	0.52	0.55	0.40
S2	0.72	0.4	0.66
S3	0.57	0.58	0.46
S4	0.56	0.57	0.47
S5	0.58	0.67	0.59
S6	0.6	0.28	0.59

As shown in Table 4, the values of n are around 0.5, denoting that the growth process is one dimensional while the rate limiting step is the diffusion of hydrogen [43]. The obtained values are consistent with that of reported by Andreasen [42], who calculated the kinetic parameters for the hydrogenation of ball-milled MgH_2-10wt.%$Mg_{17}Al_{12}$ composite. Since the n value is almost the same for all the processing conditions and there is not any considerable difference between the n values, it seems that the rate-limiting step does not change with increasing the TPCAE passes and/or processing temperature.

The calculated kinetic rate constants (Table 5), are quite consistent with those calculated by Jorge et al. [21] for an AZ91 Mg alloy after processing by ECAP under different conditions.

Table 5. Kinetic rate constants of the JMA model for the hydrogenation at different temperatures and apparent activation energy of the hydrogenation for different samples.

Sample	k_{250} [10^{-2} s^{-1}]	k_{300} [10^{-2} s^{-1}]	k_{350} [10^{-2} s^{-1}]	Apparent Activation Energy (kJ/mol)
As cast	0.08	0.69	1.7	82.9
S1	0.8	1.7	5.4	51.2
S2	0.2	4.3	1.2	48.2
S3	1.2	1.4	4.2	34.2
S4	0.6	1.7	4.3	54.9
S5	1.1	1.4	2.9	27
S6	0.6	15.9	1.6	29.8

By increasing the kinetic rate constant of the JMA model, a higher rate for nucleation and growth of transformed hydride phase is expected [21]. For the as cast sample, the kinetic rate constant decreases by one digit per each 50 °C of temperature reduction. This shows that the temperature reduction has an inverse effect on the hydrogenation kinetic for the cast alloy. For the TPCAE processed samples (with an exception of S6 sample), the kinetic rate constants for the hydrogenation at 350 °C and 300 °C, are in the same order of magnitude with a small difference, indicating that nucleation and growth rates at 300 °C are comparable to those at 350 °C, which conforms the success of TPCAE processing, to moderate the effect of lowering temperature on the nucleation and growth rates. The kinetic rate constant of hydrogenation at 300 °C for the S6 sample (fourth pass of TPCAE at 200 °C) is one order of magnitude higher than that at 350 °C, approving the effectiveness of the processing route of S6 for improvement in the hydrogenation kinetic at 300 °C. For the hydrogenation at 250 °C, S3 and S5 samples have the highest kinetic rate constants, which is attributed to the occurrence of recrystallization during the TPCAE processing that results in the grain sizes lower than 3 µm (see Table 3). Besides, for both S3 and S5 samples, the last pass of the TPCAE processing was performed at 250 °C (see Table 2), showing that the optimum TPCAE processing temperature to have an acceptable hydrogenation kinetic at low temperature is 250 °C.

In terms of the activation energies in Table 5, it is obvious that the highest amount corresponds to the cast sample. This is consistent with the obtained value of 81 kJ/mol by Andreasen [42], on the hydrogenation activation energy of ball-milled MgH_2-10 wt.%$Mg_{17}Al_{12}$ composite. The range of activation energy from 27 to 55 kJ/mol for the TPCAE processed samples shows a significant improvement in comparison to the range of 90-140 kJ/mol usually reported for the activated Mg powders [42,44], and 72 kJ/mol reported for the Mg thin films in the literature [45]. The values at the upper bound of the range correspond to the S1 and S4. The lowest activation energies are related to S5 (third pass) and S6 (fourth pass) that have the highest amount of thermomechanical processing. As mentioned, the internal defects such as the grain boundaries, the dislocations, and the precipitate interfaces facilitate the diffusion of the hydrogen atoms through the material bulk and provide nucleation sites for the formation of hydride phase, leading to the reduction of the activation energy. Therefore, the activation energy variations can be interpreted by the microstructure evolution during the TPCAE processing.

Considering all the aforementioned parameters, the highest activation energy is expected for the as cast sample, due to its largest grain size and its lowest dislocation density. After a first pass of TPCAE, grain size decreases significantly, a huge number of dislocations generate in the microstructure, and initial β-phase precipitates start to appear (Table 3), so a lower activation energy is observed.

By further processing the sample (the second pass of TPCAE), grain size decreased and the volume fraction of precipitates increased that result in a further decrease in the activation energy. However, the lowest activation energy for the second pass samples is achieved at the processing temperature of 250 °C (S3 sample) due to its lower processing temperature than the S2 sample (second pass of TPCAE at 300 °C) in which the grain growth is hindered by the lower diffusion rate of Mg atoms, and due to the more homogenous microstructure than the S4 sample (second pass of TPCAE at 200 °C), more detail of the microstructural investigations can be found in Section 3.1. By continuing the TPCAE processing to the third (S5 sample) and fourth pass (S6 sample) of the process, a finer microstructure, and a higher amount of β-phase precipitates are observed (see Table 3). A higher volume fraction of β-phase precipitates with fine dispersion, results in the higher contribution of interfaces in the diffusion of the hydrogen atoms into the material bulk [21], which would improve the diffusion of hydrogen atoms and reduction of the activation energy. Additionally, the β-phase precipitates, acting as a catalyst, reduce the H_2 dissociation energy [46], and may act as nucleation points for the hydride phase [39]. From all the above, it is expected to have a lower activation energy for the samples that have higher thermomechanical works and have their last pass of the TPCAE process at lower temperatures.

However, on the contrary to the S2 and S3 samples, the S4 sample, with the second pass of processing at 200 °C, has a relatively high activation energy as S1. The reason is that, although the processing at a low temperature of 200 °C may lead to a high amount of precipitation and dislocation density, such a sudden reduction of temperature causes a more bimodal and non-homogenous microstructure, as mentioned before, which is not effective for the reduction of activation energy. In fact, implementing a sufficient thermomechanical work while there is a step-by-step temperature reduction throughout the passes leads to form a finer microstructure with a homogenous distribution of the precipitates, playing the major role in reducing the activation energy and improving the hydrogenation kinetic. This explains the lowest activation energies for S5 sample (third pass of TPCAE at 250 °C) and S6 sample (fourth pass of TPCAE at 200 °C).

Generally, considering the absorption and desorption behavior of different samples with different conditions, it could be stated that the TPCAE processing has made a remarkable improvement on the kinetics of hydrogenation and dehydrogenation of cast AZ91 alloy, specifically when the gradual reduction of processing temperature is applied during the implementation of sufficient thermomechanical work level.

5. Conclusions

In comparison to the cast condition, significant improvements are obtained via TPCAE processing in terms of both increasing the storage capacity and kinetics of absorption/desorption. For hydrogenation, a significant improvement is achieved at 350 °C and 300 °C, but to a lower extent at 250 °C. The hydrogenation behavior at 300 °C becomes closer to the behavior at 350 °C. On the other hand, the improvement in dehydrogenation is made particularly at 350 °C. Applying sufficient level of thermomechanical work during the step-by-step temperature reduction results in the formation of a homogenous and fine-grained microstructure, including fine dispersion of β-$Mg_{17}Al_{12}$ precipitates. Therefore, due to the increase of the internal defects, which are appropriate for diffusion of hydrogen atoms, remarkable results are obtained, as below:

- The maximum storage capacity of 6.1 wt.% is obtained at a time span below 2000 s.
- The activation energy for hydrogenation is reduced from 82.9 kJ/mol to the range of 27–54.9 kJ/mol. The results show that the TPCAE processing is capable of reducing the activation energy to lower than 30 kJ/mol.

- The complete dehydrogenation is done at 350 °C in a time range of 1000 s up to maximum 2500 s.

Author Contributions: Investigation, M.A., R.E. and E.B.; writing—original draft preparation, M.A. and R.E.; formal analysis and data curation, M.A.; project administration, funding acquisition, and conceptualization, R.E.; supervision, R.E. and E.B.; writing—review and editing, E.B. All authors have read and agreed to the published version of the manuscript.

Funding: This research was funded by SHIRAZ UNIVERSITY, grant number 99-GR-ENG 15.

Conflicts of Interest: The authors declare no conflict of interest. The funders had no role in the design of the study; in the collection, analyses, or interpretation of data; in the writing of the manuscript; or in the decision to publish the results.

References

1. Varin, R.A.; Czujko, T.; Wronski, Z.S. *Nanomaterials for Solid State Hydrogen Storage*; Springer Science & Business Media: New York, NY, USA, 2009; pp. 3–5. [CrossRef]
2. Schlapbach, L.; Züttel, A. Hydrogen-storage materials for mobile applications. In *Materials for Sustainable Energy: A Collection of Peer-Reviewed Research and Review Articles from Nature Publishing Group*; World Scientific: Singapore, 2011; pp. 265–270. [CrossRef]
3. Yang, Y.; Xiong, X.; Chen, J.; Peng, X.; Chen, D.; Pan, F. Research advances in magnesium and magnesium alloys worldwide in 2020. *J. Magnes. Alloys* **2021**, *9*, 705–747. [CrossRef]
4. Huot, J.; Liang, G.; Boily, S.; Van Neste, A.; Schulz, R. Structural study and hydrogen sorption kinetics of ball-milled magnesium hydride. *J. Alloys Compd.* **1999**, *293*, 495–500. [CrossRef]
5. Song, M.; Lee, J.Y. A study of the hydriding kinetics of Mg-(10–20 w/o) LaNi5. *Int. J. Hydrogen Energy* **1983**, *8*, 363–367. [CrossRef]
6. Soyama, J.; Triques, M.R.M.; Leiva, D.R.; Junior, A.M.J.; da Silva, E.P.; Pinto, H.C.; Bolfarini, C.; Kiminami, C.S.; Botta, W.J. Hydrogen storage in heavily deformed ZK60 alloy modified with 2.5 wt.% Mm addition. *Int. J. Hydrogen Energy* **2016**, *41*, 4177–4184. [CrossRef]
7. Huang, S.-J.; Chiu, C.; Chou, T.-Y.; Rabkin, E. Effect of equal channel angular pressing (ECAP) on hydrogen storage properties of commercial magnesium alloy AZ61. *Int. J. Hydrogen Energy* **2018**, *43*, 4371–4380. [CrossRef]
8. Li, X.; Lin, Y. Influence of Al doping on stability of Mg1− xTix and their hydrides. *Acta Phys. Sin.* **2013**, *62*, 138801. [CrossRef]
9. Au, M. Hydrogen storage properties of magnesium based nanostructured composite materials. *Mater. Sci. Eng. B* **2005**, *117*, 37–44. [CrossRef]
10. Leiva, D.R.; Fruchart, D.; Bacia, M.; Girard, G.; Skryabina, N.; Villela, A.C.; Miraglia, S.; Santos, D.S.; Botta, W.J. Mg alloy for hydrogen storage processed by SPD. *Int. J. Mater. Res.* **2009**, *100*, 1739–1746. [CrossRef]
11. Zaluski, L.; Zaluska, A.; Tessier, P.; Strom-Olsen, J.; Schulz, R. Nanocrystalline hydrogen absorbing alloys. In Proceedings of the Materials Science Forum, 10 July 1996; p. 2. [CrossRef]
12. Révész, Á.; Gajdics, M.; Schafler, E.; Calizzi, M.; Pasquini, L. Dehydrogenation-hydrogenation characteristics of nanocrystalline Mg_2Ni powders compacted by high-pressure torsion. *J. Alloys Compd.* **2017**, *702*, 84–91. [CrossRef]
13. Skripnyuk, V.; Rabkin, E.; Bendersky, L.; Magrez, A.; Carreño-Morelli, E.; Estrin, Y.J. Hydrogen storage properties of as-synthesized and severely deformed magnesium–multiwall carbon nanotubes composite. *Int. J. Hydrogen Energy* **2010**, *35*, 5471–5478. [CrossRef]
14. Khani, S.; Salehi, M.; Samim, H.; Aboutalebi, M.; Palkowski, H. The effect of severe plastic deformation on the microstructure and mechanical properties of as-cast AZ31. *Iran. J. Mater. Sci. Eng.* **2016**, *13*, 29–38.
15. Malik, A.; Wang, Y.; Nazeer, F.; Khan, M.A.; Ali, T.; Ain, Q.T. Effect of pre-straining on twinning, texture and mechanical behavior of magnesium alloys A-review. *J. Mater. Res. Technol.* **2020**, *9*, 14478–14499. [CrossRef]
16. Skripnyuk, V.; Rabkin, E.; Estrin, Y.; Lapovok, R. Improving hydrogen storage properties of magnesium based alloys by equal channel angular pressing. *Int. J. Hydrogen Energy* **2009**, *34*, 6320–6324. [CrossRef]
17. Chiu, C.; Huang, S.-J.; Chou, T.-Y.; Rabkin, E. Improving hydrogen storage performance of AZ31 Mg alloy by equal channel angular pressing and additives. *J. Alloys Compd.* **2018**, *743*, 437–447. [CrossRef]
18. Jorge, A.M., Jr.; Prokofiev, E.; de Lima, G.F.; Rauch, E.; Veron, M.; Botta, W.J.; Kawasaki, M.; Langdon, T.G. An investigation of hydrogen storage in a magnesium-based alloy processed by equal-channel angular pressing. *Int. J. Hydrogen Energy* **2013**, *38*, 8306–8312. [CrossRef]
19. Edalati, K.; Yamamoto, A.; Horita, Z.; Ishihara, T. High-pressure torsion of pure magnesium: Evolution of mechanical properties, microstructures and hydrogen storage capacity with equivalent strain. *Scr. Mater.* **2011**, *64*, 880–883. [CrossRef]
20. Hongo, T.; Edalati, K.; Arita, M.; Matsuda, J.; Akiba, E.; Horita, Z. Significance of grain boundaries and stacking faults on hydrogen storage properties of Mg_2Ni intermetallics processed by high-pressure torsion. *Acta Mater.* **2015**, *92*, 46–54. [CrossRef]
21. Jorge, A.M., Jr.; Prokofiev, E.; Triques, M.R.M.; Roche, V.; Botta, W.J.; Kiminami, C.S.; Raab, G.I.; Valiev, R.Z.; Langdon, T.G. Effect of cold rolling on the structure and hydrogen properties of AZ91 and AM60D magnesium alloys processed by ECAP. *Int. J. Hydrogen Energy* **2017**, *42*, 21822–21831. [CrossRef]

22. Skripnyuk, V.; Buchman, E.; Rabkin, E.; Estrin, Y.; Popov, M.; Jorgensen, S. The effect of equal channel angular pressing on hydrogen storage properties of a eutectic Mg–Ni alloy. *J. Alloys Compd.* **2007**, *436*, 99–106. [CrossRef]
23. Skripnyuk, V.; Rabkin, E.; Estrin, Y.; Lapovok, R. The effect of ball milling and equal channel angular pressing on the hydrogen absorption/desorption properties of Mg–4.95 wt.% Zn–0.71 wt.% Zr (ZK60) alloy. *Acta Mater.* **2004**, *52*, 405–414. [CrossRef]
24. Asselli, A.; Leiva, D.; Huot, J.; Kawasaki, M.; Langdon, T.; Botta, W. Effects of equal-channel angular pressing and accumulative roll-bonding on hydrogen storage properties of a commercial ZK60 magnesium alloy. *Int. J. Hydrogen Energy* **2015**, *40*, 16971–16976. [CrossRef]
25. Botta, W.; Jorge, A., Jr.; Veron, M.; Rauch, E.; Ferrie, E.; Yavari, A.; Huot, J.; Leiva, D. H-sorption properties and structural evolution of Mg processed by severe plastic deformation. *J. Alloys Compd.* **2013**, *580*, S187–S191. [CrossRef]
26. Jorge, A.M., Jr.; de Lima, G.F.; Triques, M.R.M.; Botta, W.J.; Kiminami, C.S.; Nogueira, R.P.; Yavari, A.R.; Langdon, T.G. Correlation between hydrogen storage properties and textures induced in magnesium through ECAP and cold rolling. *Int. J. Hydrogen Energy* **2014**, *39*, 3810–3821. [CrossRef]
27. Huot, J.; Skryabina, N.Y.; Fruchart, D. Application of severe plastic deformation techniques to magnesium for enhanced hydrogen sorption properties. *Metals* **2012**, *2*, 329–343. [CrossRef]
28. Abdi, M.; Ebrahimi, R. Twin parallel channel angular extrusion as a development of ECAE in parallel channels. *SN Appl. Sci.* **2020**, *2*, 1–10. [CrossRef]
29. Schneider, C.A.; Rasband, W.S.; Eliceiri, K.W. NIH Image to ImageJ: 25 years of image analysis. *Nat. Methods* **2012**, *9*, 671–675. [CrossRef] [PubMed]
30. Abdi, M.; Ebrahimi, R. Microstructure Evolution of AZ91 Alloy Processed by Twin Parallel Channel Angular Extrusion Technique. *J. Mater. Eng. Perform.* **2022**, *31*, 5358–5373. [CrossRef]
31. Asselli, A.A.C.; Hébert, N.B.; Huot, J. The role of morphology and severe plastic deformation on the hydrogen storage properties of magnesium. *Int. J. Hydrogen Energy* **2014**, *39*, 12778–12783. [CrossRef]
32. Dini, H.; Svoboda, A.; Andersson, N.-E.; Ghassemali, E.; Lindgren, L.-E.; Jarfors, A.E. Optimization and validation of a dislocation density based constitutive model for as-cast Mg-9% Al-1% Zn. *Mater. Sci. Eng. A* **2018**, *710*, 17–26. [CrossRef]
33. Khani, S.; Aboutalebi, M.; Salehi, M.; Samim, H.; Palkowski, H. Microstructural development during equal channel angular pressing of as-cast AZ91 alloy. *Mater. Sci. Eng. A* **2016**, *678*, 44–56. [CrossRef]
34. Wang, Q.; Chen, Y.; Liu, M.; Lin, J.; Roven, H.J. Microstructure evolution of AZ series magnesium alloys during cyclic extrusion compression. *Mater. Sci. Eng. A* **2010**, *527*, 2265–2273. [CrossRef]
35. Yuan, Y.; Guo, Q.; Sun, J.; Liu, H.; Xu, Q.; Wu, Y.; Song, D.; Jiang, J.; Ma, A. High mechanical properties of AZ91 Mg alloy processed by equal channel angular pressing and rolling. *Metals* **2019**, *9*, 386. [CrossRef]
36. Peng, W.; Lan, Z.; Wei, W.; Xu, L.; Guo, J. Investigation on preparation and hydrogen storage performance of $Mg_{17}Al_{12}$ alloy. *Int. J. Hydrogen Energy* **2016**, *41*, 1759–1765. [CrossRef]
37. Jia, Y.; Sun, C.; Shen, S.; Zou, J.; Mao, S.S.; Yao, X. Combination of nanosizing and interfacial effect: Future perspective for designing Mg-based nanomaterials for hydrogen storage. *Renew. Sustain. Energy Rev.* **2015**, *44*, 289–303. [CrossRef]
38. Floriano, R.; Leiva, D.; Melo, G.; Ishikawa, T.; Huot, J.; Kaufman, M.; Figueroa, S.; Mendoza-Zélis, L.A.; Damonte, L.C.; Botta, W. Low temperature rolling of AZ91 alloy for hydrogen storage. *Int. J. Hydrogen Energy* **2017**, *42*, 29394–29405. [CrossRef]
39. Amira, S.; Huot, J. Effect of cold rolling on hydrogen sorption properties of die-cast and as-cast magnesium alloys. *J. Alloys Compd.* **2012**, *520*, 287–294. [CrossRef]
40. Hui, J.; Zhang, X.; Liu, T.; Liu, W.; Wang, B. First-principles calculation of twin boundary energy and strength/embrittlement in hexagonal close-packed titanium. *Mater. Des.* **2022**, *213*, 110331. [CrossRef]
41. Töpler, J.; Buchner, H.; Säufferer, H.; Knorr, K.; Prandl, W. Measurements of the diffusion of hydrogen atoms in magnesium and Mg_2Ni by neutron scattering. *J. Less Common Met.* **1982**, *88*, 397–404. [CrossRef]
42. Andreasen, A. Hydrogenation properties of Mg–Al alloys. *Int. J. Hydrogen Energy* **2008**, *33*, 7489–7497. [CrossRef]
43. Karty, A.; Grunzweig-Genossar, J.; Rudman, P. Hydriding and dehydriding kinetics of Mg in a Mg/Mg_2Cu eutectic alloy: Pressure sweep method. *J. Appl. Phys.* **1979**, *50*, 7200–7209. [CrossRef]
44. Galey, B.; Auroux, A.; Sabo-Etienne, S.; Dhaher, S.; Grellier, M.; Postole, G. Improved hydrogen storage properties of Mg/MgH_2 thanks to the addition of nickel hydride complex precursors. *Int. J. Hydrogen Energy* **2019**, *44*, 28848–28862. [CrossRef]
45. Johansson, M.; Ostenfeld, C.W.; Chorkendorff, I. Adsorption of hydrogen on clean and modified magnesium films. *Phys. Rev. B* **2006**, *74*, 193408. [CrossRef]
46. Crivello, J.-C.; Nobuki, T.; Kato, S.; Abe, M.; Kuji, T. Hydrogen absorption properties of the γ-$Mg_{17}Al_{12}$ phase and its Al-richer domain. *J. Alloys Compd.* **2007**, *446*, 157–161. [CrossRef]